AEMR
Advances in Energy and Materials Research
https://jaem.qom.ac.ir/

Synthesis of $Yb_2V_2O_7$ nanomaterials for catalytic fabrication of 2-amino-4H-chromene compounds under microwave irradiations

Shahin Khademinia

1 Department of Inorganic Chemistry, Faculty of Chemistry, Semnan University, Semnan, Iran. Email: khademiniashahin@gmail.com

Article Info

Article type:
Research Article

Article history:
Received 2 Jan 2024
Received in revised form 1 Mar 2024
Accepted 27 Apr 2024
Published online 24 Jun 2024

Keywords:
$Yb_2V_2O_7$, Nanomaterial, Solid State Method, Chromene, Microwave.

ABSTRACT

Synthesis of Yb2V2O7 nano-powders was reported by solid state reactions using Yb2O3 and Na2VO4 at stoichiometric 1:1 Yb:V molar ratio as raw materials for the first time. Powder X-ray diffraction (PXRD) technique was used to characterize the as-prepared nanomaterials. Crystal phase change due to changing the reaction time was studied by FullProf program. The results showed that the patterns had a main cubic Yb2V2O7 crystal structure with a space group of $Fd\bar{3}m$. As could be found from the XRD data, the synthesized Yb2V2O7 sample was stable at the reaction temperature until 400 ºC. It was found that increasing the reaction temperature had a reverse effect on the stability and so purity of the synthesized samples. FESEM images showed that the synthesized Yb2V2O7 particles had sphere morphology with homogeneity in size and morphology. Ultraviolet–visible spectroscopy (UV-Vis) analysis showed that the synthesized Yb2V2O7 nanopowder had strong light absorption property in the ultraviolet-visible light region. The catalytic performance of the synthesized Yb2V2O7 nanomaterial was studied for the fabrication of 2-amino-4H-chromene compounds under solvent condition. The reaction parameters affect on the reaction yield such as reaction time, solvent type and catalyst amount were studied. The maximum yield for the synthesis of the Chromene compounds was obtained (94%) when H2O was used as reaction solvent, the catalyst amount, reaction time and temperature, and illumination frequency were (10 mol%), 12 min, 70 ˚C and 50 kHz, respectively, while benzaldehyde was used as aldehyde derivative.

Cite this article: Khademinia, Sh. & Samadi, Sh. (2024). Synthesis of Yb2V2O7 nanomaterials for catalytic fabrication of 2-amino-4H-chromene compounds under microwave irradiations, *Advances in Energy and Materials Research*, 1 (2), 1-10. https://doi.org/10.22091/jaem.2025.10853.1011

DOI: https://doi.org/10.22091/jaem.2025.10853.1011
Publisher: University of Qom.

1. Introduction

Pyrochlore materials with general formula $A_2B_2O_7$ are related to the fluorite structure and the nature of this relationship is discussed in the crystallography of this compounds [1]. There are few compounds that have simultaneously ferromagnetic and semiconductor properties. One of the compounds is $Yb_2V_2O_7$. Rare earth ortho vanadates are important class of inorganic functional materials studied extensively for their structural and chemical properties. $Yb_2V_2O_7$ has pyrochlore type structure. According to reported researches conducted on $Yb_2V_2O_7$ materials, it has been found that $Yb_2V_2O_7$ crystallizes in cubic crystal system with space group $Fd\bar{3}m$. These compounds have unique physical properties such as catalysis [2-5], electronic [6], magnetic properties [7,8], optical properties [9] and are applied in solid oxide fuel cells (SOFC) [10]. Also, the compound has the ferromagnetic property with the highest value of $T_{C,}$ so they can be ideal option for use on different device from computer to high temperature sensors. There is a major magnetic data have been reported for $Yb_2V_2O_7$ nanomaterials [11,12]. Some routes are introduced for the preparation of $Yb_2V_2O_7$ nanomaterials such as solid state using VO_2 and Yb_2O_3 [13], floating – zone [14-16], and heating $REVO_4$ [17], flux growth [18-20], hydrothermal [21], liquid – phase [22, 23], melt-mode [24], precipitation [25], pressing the sample to 25 GPa and aging at room temperature [26] and solid-phase synthesis [27]. Chromene compounds are heterocycles chief components of many naturally produced products. Basically, Chromene compounds are interested because of their uses as cosmetic agents, food additives, and potential biodegradable agrochemicals. Besides, Chromene compounds show several pharmacological activities such as anticancer, anticoagulant, anti-HIV, diuretic, antimalarial, antitumor, antibacterial, antileukemic, antimalarial, and antianaphylactic applications. Also, Chromene materials are components of various naturally produces products like calanone, calanolides, and calophyllolides. Moreover, the compounds are used in several diseases such as cognitive enhancers for the treatment of neurodegenerative disease, including amyotrophic lateral sclerosis, Alzheimer's disease, Parkinson's disease, Huntington's disease, AIDS-associated dementia, and down syndrome as well as for the treatment of myoclonus and schizophrenia [28-30]. The microwave portion of electromagnetic radiation is emerged a significant area in the acceleration of chemical reactions. There are three main reasons for its special place of microwave (MW) assisted synthesis. The first point is high heating efficiency caused by MW energy, which reaches and absorbed directly by substance. The second is selectivity i.e. having dielectric polar molecule will absorb this energy. And thirdly enhancement of chemical syntheses by the MW effect or non-thermal effect. In other sense, the microwave irradiation energy acts as internal heat source, which is able to heat the target compounds without heating the entire furnace or oil bath, consequently, saves time and energy. It produces more uniform heating. In this regard Microwave heating technique has blossomed in a variety of applications in Organic Synthetic methods. Although the initial synthetic work was performed in domestic Microwave ovens but recently most organic reactions are carried out in dedicated high speed specialized Microwave equipment with appropriate pressure and temperature control. Besides, organic/inorganic hybrid functional materials. In this process, a direct reaction in one step is used for the preparation of inorganic parts while the organic component works as surface capping material or template [31-33]. For the mentioned reasons, we used microwave energy source and one-pot method for the fabrication of Chromene compounds.

In the present work, solid state method is used for the synthesis of $Yb_2V_2O_7$ nanostructures. Crystalline phase growth of the synthesized materials in different conditions is investigated using Rietveld analysis. Physical properties of the fabricated samples are investigated by FESEM, (UV-Vis) spectroscopy, BET and BJH methods. Besides, the performance of the synthesized samples for the preparation of Chromene derivatives is investigated.

2. Experimental

2.1. Materials and instruments

Yb_2O_3, Na_3VO_4, aromatic aldehyde derivative, malononitrile, β-naphtol and the used solvents were purchased from commercial sources (Merck and Sigma Aldrich Companies) with synthesis grade and used without further purifications. The crystal structure of as-prepared materials was recorded on a X-ray diffraction (XRD, Ultima IV, Rigaku) with Cu-Kα radiation at a scan rate of $0.1^{o}\cdot s^{-1}$ with 2θ degree range from 10^{o} to 80^{o}. Rietveld analysis was performed by *FullProf* software. A field emission scanning electron microscope (Hitachi FE-SEM model S-4160) was used to determine the morphology of the obtained samples. The fabricated sample was dispersed in water and cast onto a copper grid to study the size and morphology of the synthesized materials by TEM (Transmission Electron Microscope) using a Philips – CM300 - 150 KV microscope. BET and BJH data were collected on a Beckman Coulter SA3100 Surface Area Analyzer. Ultraviolet (UV)–visible spectra were acquired with U-3900H Spectrophotometer (Hitachi). Microwave irradiation was applied by a Yusch Heating Microwave oven (1000 W) under atmospheric pressure.

2.2. Solid State synthesis of $Yb_2V_2O_7$ nanomaterial

In a typical synthesis experiment, 0.5 mmol of Yb_2O_3 (M_W = 394.08 g mol^{-1}) and 1 mmol of Na_3VO_4 (M_w = 183.907 g mol^{-1}) with Yb:V molar ratio of 1:1 were ground in a mortar until an almost homogenous powder was obtained. A 25 mL crucible was used as a container for the obtained powder. The contained powder crucible was transferred into an electric furnace that had already reached to a desired temperature at S_1= 300, S_2 = 400℃, S_3 = 500℃, and S_4 = 600℃ and treated thermally for 8 h. The crucible was then allowed to cool down to the room temperature in the furnace.

2.3. General remarks to fabricate 2-amino-4H-chromene compounds

In a typical experiment, aromatic aldehyde derivative (**1**, 1 mmol), malononitrile (**2**, 1 mmol), β-naphtol (**3**, 1 mmol) and nanocatalyst (10 mol%) were mixed in a 5 mL solvent and putted into a microwave oven. The reaction mixture was illuminated by the microwave radiation for a certain time (for example 12 min) until the reaction was completed. The completion of the reaction was confirmed by TLC (Ethyl acetate:n-Hexane 4:6). When the reaction was completed, 10 mL of hot ethanol was added to the reaction mixture to dissolve the product and filter the nanocatalyst. To separate the catalyst, the alcoholic mixture was poured onto a Buchner funnel covered by a Whatman filter paper until the fine solution was passed and the catalyst was marinated on the filter paper. Chromene product was recovered by the alcohol evaporation and recrystallized in ethanol.

3. Results and Discussion

3.1. Characterization

The phase identification of the synthesized nanomaterials was performed by powder X-ray diffraction technique. Figure 1 shows the XRD analysis of the obtained samples in the 2θ range of 10-90° associated with the structural analyses done by the *FullProf* program. Profile matching mode in Rietveld analysis with constant scale factors was used to identify the crystal phase type and growth of the obtained samples. The observed intensities are shown by red lines; The calculated data are indicated by black lines; the blue lines are the difference between the observed and calculated lines. The Bragg positions shown by blue bars are corresponded to the cubic phase of $Yb_2V_2O_7$. The Rietveld data indicate that the PXRD patterns of the synthesized compounds at the reaction temperatures in the range of 300 to 600 °C are related to main cubic $Yb_2V_2O_7$ crystal structure with space group $Fd\bar{3}m$ [11, 12, 14]. It is clear that the reaction temperature is a key factor affected the crystal phase compositio. The impurity phases revealed in the product mixture V_2O_5 (red bar) (3%) and Yb_2O_3 (green bar) (16%). The amounts of Yb_2O_3 in the product mixture are 4, 6, 9, and 16% for S_1, S_2, S_3 and S_4, respectively.

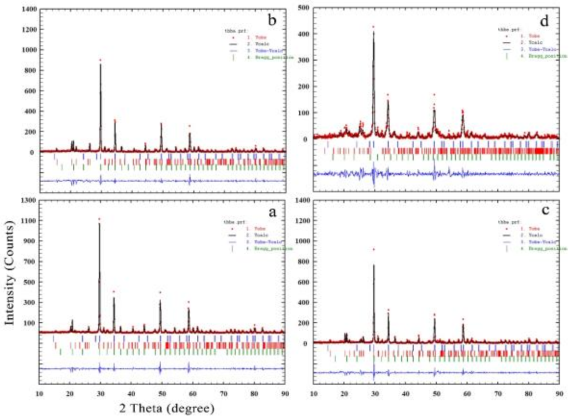

Figure 1. XRPD patterns associated with Rietveld analysis of a) S_1, b) S_2, c) S_3 and d) S_4.

The PXRD patterns of the fabricated samples reveal that a cubic $Yb_2V_2O_7$ crystal structure is obtained by heat treatment the raw materials up to 600 ° C. The crystallite size values of the synthesized compounds calculated by Scherrer equation (equation 1) at different reaction temperatures are included in table 1. Also, interplanar spacing was measured by Bragg's law ($\boldsymbol{n\lambda = 2d\sin(\theta)}$). The data included in table 1 reveal that increase in the reaction temperature, decreases the crystal growth and purity of the synthesized samples.

$$\boldsymbol{D}\ (\text{nm}) = K\lambda/B_{hkl}\cos\theta \qquad (1)$$

The dislocation density (δ) value is calculated by the below relationship. The amount is corresponded to crystal defects values.

$$\delta = \frac{1}{D^2} \qquad (2)$$

The data presented in table 1 showed that δ decreased by increase in the reaction temperature that was due to the improvement of the crystal nature of the obtained sample. So, the change in the δ value is because of the change in D value of the synthesized material because of the change in the reaction condition.

The strain (ε) value obtained by the below formula is a function of the purity of the synthesized material. The value of the parameter is included in table 1. The data presented in table 1 indicate that the reaction temperature affects on the crystallite size, strain and dislocation density values.

$$\varepsilon = \frac{\beta_{hkl}\cos\theta}{4} \qquad (3)$$

Table 1. Crystallographic parameters data for $Yb_2V_2O_7$ nanomaterials.

Data	2θ	θ	$B_{1/2}$ (°)	$B_{1/2}$ (rad)	$\cos\theta_B$	D (nm)	δ	ε	Counts
S_1	29.65	14.82	0.19	0.0037	0.9667	40	0.000625	0.894198	1100

S_2	29.70	14.85	0.38	0.0066	0.9665	23	0.001890	1.594725	900
S_3	29.65	14.82	0.32	0.0023	0.9667	24	0.001736	0.555853	850
S_4	29.58	14.79	0.38	0.0057	0.9668	24	0.001736	1.37769	450

R_f, R_B and χ^2 values included in table 2 confirm the goodness of the fittings. The reaction temperature is the main factor on the crystal phase growth and the purity of the obtained materials. It is clear that when the reaction temperature is increased to 600 ºC, the phase purity is decreased (S_1-S_4).

Table 2. Lattice parameter and interplanar spacing (d) data for $Yb_2V_2O_7$ nanomaterials.

Sample	a (Å)	R_f	R_b	χ^2	Count	d(Å)	phase purity (%)
S_1	10.427138	1.8	1.9	1.9	1114	3.01	85
S_2	10.431505	1.9	2.6	1.9	900	3.00	84
S_3	10.427916	2.3	1.7	1.9	915	3.00	82
S_4	10.449037	1.1	1.5	2.1	427	3.02	80

3.2. BET and BJH analysis

The surface area, average pore size and average pore volume data of the as-prepared samples are studied by BET and BJH analysis. The samples were degassed at 170 °C for 100 min in the nitrogen atmosphere before starting the N_2-physical adsorption measurement. By doing the experiment, the specific surface area (S_{BET}) of the obtained materials was determined by adsorption-desorption isotherms of N_2 at 77 K. The surface area, pore volume and average pore diameter of the synthesized $Yb_2V_2O_7$ nanomaterials are presented in table 3. According to table 3, it is found that the average surface area and pore volumes are about 5.9016 $m^2\ g^{-1}$ and 0.06651 $cm^3\ g^{-1}$ for S_3, 4.2351 and 0.0612 $cm^3\ g^{-1}$ for S_4. Also, the average nanoparticles sizes are 45 and 57 nm for S_3 and S_4, respectively. The BET data show that the specific surface area, and pore volume of the synthesized nanomaterials decreases by increase the reaction temperature. Also, the textural properties of the as-prepared materials are also included in table 4. The data summarized in table 4 shows that the specific surface area and pore volume and pore size of S_3 is more than the other samples. The observations of the BET and BJH measurements suggest that the surface area of S_3 is more than the other samples.

Table 3. Surface area, pore volume and average particle size for $Yb_2V_2O_7$ samples obtained by BET method.

Sample	BET surface area (m^2g^{-1})	Pore volume (cm^3g^{-1})	Average particles size (nm)
S_3	5.9016	0.066514	45.082
S_4	4.2351	0.061208	57.811

Table 4. Surface area, pore volume and average pore sizes for $Yb_2V_2O_7$ samples obtained by BJH method.

Property	S_3	S_4
surface area of pores	6.3745	4.0091
volume of pores	0.0668	0.0611
average pore width (4V/A)	41	61

3.3. Morphology analysis

FESEM images of the as-synthesized $Yb_2V_2O_7$ compounds are shown in figures 3. İt is obvious in figure 3 a that when the reaction temperature is 300 °C, the morphology of this materials is sponge. İt is indicated that the diameter size of the particles formed the sponge are in the range of 30 - 80 nm. Figure 3b show FESEM image of sample S_2. The image shows that the morphology of the obtained material is sponge. Besides, TEM image of S_1 is also presented in figure 3. It shows that the oparticle sizes are about 40 to 90 nm.

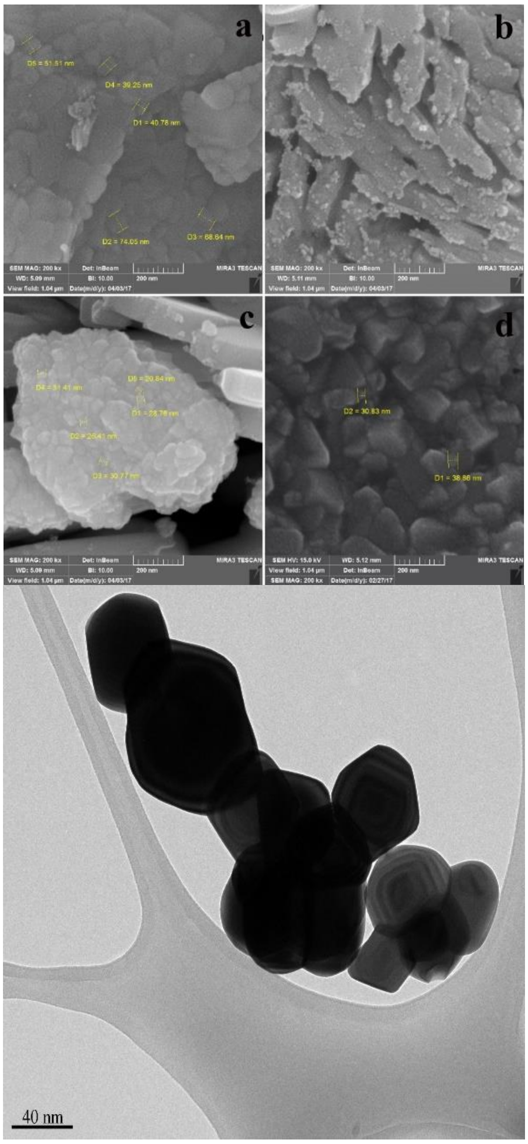

Figure 3. FESEM images of a) S_1, b) S_2, c) S_3, d) S_4, and e) TEM image of S_1.

3.4. Optical properties

Figurs 4 shows the Eg data of the synthesized $Yb_2V_2O_7$ samples. The optical direct band gap energies of the synthesized samples were obtained by the relation $(\alpha h\nu)^2 = A(h\nu - Eg)$, where A and Eg are a constant and the direct band gap energy, respectively [34]. The Eg values were obtained from extrapolating the linear part of the curve to the hυ axis. The Eg values of the $Yb_2V_2O_7$ nanomaterials were in the range of 2.4 to 4.5

eV for S_1 to S_4, respectively. As could be found from the data, Yb_2O_3 and V_2O_5 band gap energy values are about 4.9 eV [35] and 1.7 eV [36], respectively. So, it can be concluded that the increase in Eg value can be due to increase in Yb_2O_3 proportion in the product mixture.

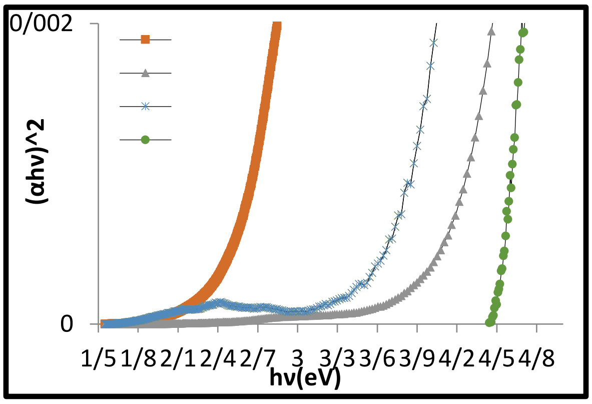

Figure 4. Plots of Eg values for a) S_1, b) S_2, c) S_3, d) S_4.

3.5. Catalytic study

The fabrication of 2-amino-4H-chromene compounds under microwave irradiation by the as-prepared $Yb_2V_2O_7$ nanocatalyst is presented in the current work. Some reaction parameters affecting on the Chromene production yield including catalyst amount, reaction time and solvent type were studied to obtain the maximum yield. Scheme 1 presents the reaction pathway for the fabrication of the Chromene compounds. The reaction yield was 94% when R=H, H_2O is solvent, at 70 °C for 12 min by using 10 mol% catalyst.

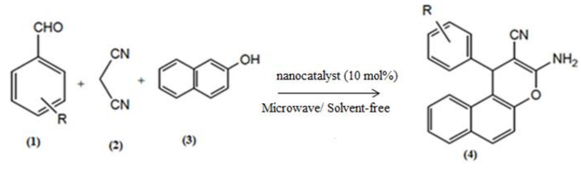

R = H , 2-Cl , 3-Cl , 4-Cl , 4-Br , 4-F , 4-Me , 3-OMe , 4-OMe , 3-NO_2 , 4-NO_2 , 3-OH , 4-OH

Scheme 1. Catalytic reaction rout for the fabrication of Chromene compounds by $Yb_2V_2O_7$ nanostructure.

The reaction time, temperature and solvent type effects on the Chromene reaction yield are studied in figure 5 a-d. The data presented in figure 5 a show that the reaction time and temperature and irradiation frequency are 12 min, 70 ˚C and 50 kHz. It was found that the maximum yield is obtained when 10 mol% of the $Yb_2V_2O_7$ was used as catalyst in the Chromene reaction mixture. The effect of solvent type on the Chromene reaction yield is presented in figure 5 b. The observation shows that the maximum reaction yield is achieved when H_2O is used as reaction solvent. However, it is clear that the reaction yield is about zero when the solvent free condition is applied and or $CHCl_3$ and or $(C_2H_5)_2O$ are used as the reaction solvent. The reusability property of $Yb_2V_2O_7$ nanocatalyst in the Chromene reaction is presented in figure 5 c. The reaction kinetic study of the present Chromene reactions is important part to study the effect of the parameters on the reaction rate. The kinetic data indicate that the linear dependence of the graphs at the time range among 0 to 25 min follows a first-order kinetic model for the two samples. The slope of the line shows the apparent rate constant (K_{app}). The amounts of K_{app} and R^2 are 0.126 min^{-1} and 0.957, under microwave irradiation (figure 5 d).

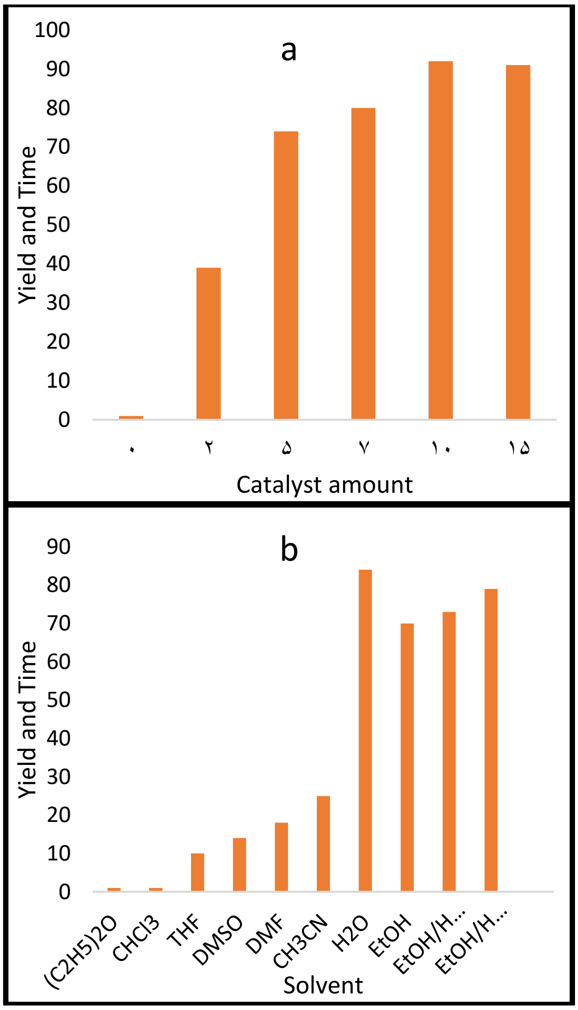

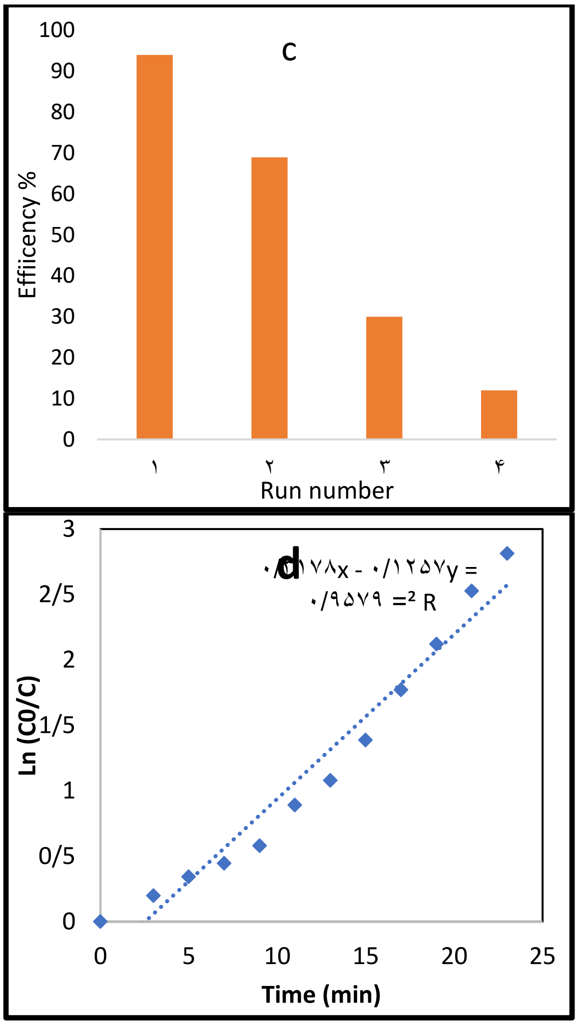

Figure 5. a) Plot of Catalyst amount effect on the reaction yield at 70 ºC for 12 min, b) Solvent type effect on the reaction yield at (10 mol%) and 70 ˚C for 12 min, c) Reusability of $Yb_2V_2O_7$ nanocatalyst at (10 mol%) and 70 ˚C for 12 min, **d)** Plot of ln (C_0/C) versus reaction time for the fabrication of Chromene compounds. Reaction condition: aldehyde **1 (R = H)** (1 mmol), malononitrile **2** (1 mmol), β-naphtol **3** (1 mmol), nanocatalyst (10 mol%).

3.6. Mechanism

A plausible reaction mechanism for the synthesis of 2-amino-4H-chromenes is shown in Scheme 1. Firstly, aldehyde (1) is activated by catalyst to generate 2-arylidenemalononitrile (3), which is formed by Knoevenagel condensation of the activated aldehyde with malononitrile (2). When 2-arylidenemalononitrile is activated by catalyst, it undergone nucleophilic attack by β-naphthol (4) to generate activated intermediate (5), which is simultaneously aromatized (6), activated, undergoes Michael cyclization (7) and the catalyst is recovered to give the product (8).

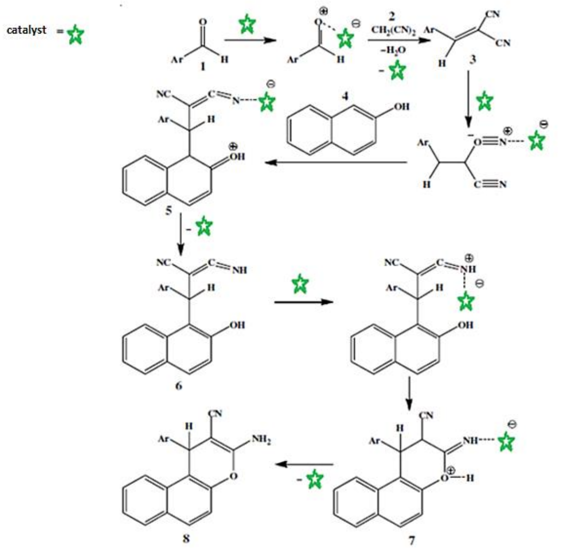

Scheme 1. A plausible reaction mechanism for the synthesis of 2-amino-4*H*-chromenes.

The reaction yields associated with the measured melting point of the recrystallized products are presented in table 5. The values of the reaction yields reveal that the maximum yield is observed when R=H, 2-NO_2 and 4-NO_2. It is found that when the aldehyde compounds are electron withdrawing group, the maximum reaction yield is obtained. Besides, it is found that the reaction time for the mentioned groups is below 20 min showing the proper reaction rate at the conditions.

Table 5. Fabrication of Chromene compounds using 10 mol% $Yb_2V_2O_7$ nanocatalyst at 70 ºC.

Entry	R	Yield(%)/Time(min)	Observed m.p.(˚C)	Reported m.p.(˚C)
1	H	94/12	279	278-280[37]
2	2-Cl	88/18	262	259-261[38]
3	3-Cl	93/18	212	211-213[39]
4	4-Cl	92/18	210	208-210[40]
5	4-Br	91/20	241	241-243[41]
6	4-F	90/19	234	232-234[42]
7	4-Me	88/35	183	182-184[43]
8	3-OMe	85/30	166	162-164[44]
9	4-OMe	87/40	181	182-183[45]
10	3-NO_2	312	233	232-234[46]
11	4-NO_2	93/15	188	188-190 [47]
12	3-OH	81/35	283	281-283[47]
13	4-OH	80/40	292	290-292[47]

3.7. FTIR and NMR Spectroscopies analyses

The FTIR and NMR spectroscopies analyses data of some of the prepared organic compounds are given below:

3-Amino-1-phenyl-1*H*-benzo[*f*]chromene-2-carbonitrile (Entry 1):

White solid; M.p. 279 ºC; IR (KBr, *v*, cm^{-1}): 3455, 3351, 2183, 1669, 1600, 1539, 1502, 1193, 1080; ^1H NMR (DMSO-d_6): δ 7.93–7.85 (m, 2H, ArH), 7.84 (d, $J = 6.2$ Hz, 1H, ArH), 7.45–7.15 (m, 8H, ArH), 6.97 (bs, 2H, NH_2), 5.30 (s, 1H, CH); CHN ($C_{20}H_{14}N_2O$) calc. (%):

C (80.53), H (4.69), N (9.39); found (%): C (80.36), H (4.57), N (9.22).

3-Amino-1-(2-chlorophenyl)-1*H*-benzo[*f*]chromene-2-carbonitrile (Entry 2):

White solid; M.p. 262 °C; IR (KBr, *v*, cm^{-1}): 3433, 3350, 2181, 1664, 1608, 1571, 1520, 1507, 1325, 1272, 1066, 768; ^{1}HNMR (DMSO-d_6): δ 5.72 (s, 1H, CH), 6.97 (s, 1H, ArH), 7.00 (s, 2H, NH_2), 7.14 (t, J = 3.0 Hz, 2H, ArH), 7.31 (d, J = 8.1 Hz, 1H, ArH), 7.35–7.42 (m, 3H, ArH) 7.63 (d, J = 8.0 Hz, 1H, ArH), 7.92–7.98 (m, 2H, ArH); CHN ($C_{20}H_{13}ClN_2O$) calc. (%): C (72.18), H (3.90), N (8.42); found (%): C (72.09), H (3.65), N (8.13).

3-Amino-1-(3-chlorophenyl)-1*H*-benzo[*f*]chromene-2-carbonitrile (Entry 3):

White solid; M.p. 212 °C; IR (KBr, *v*, cm^{-1}): 3439, 3356, 2180, 1662, 1600, 1575, 1523, 1500, 1321, 1271, 1064, 760; ^{1}HNMR (DMSO-d_6): δ 8.02 (s, 1H, ArH), 8.00 (d, *J* = 8.1 Hz, 1H, ArH), 7.97 (d, *J* = 7.8 Hz, 1H, ArH), 7.94 (d, *J* = 7.6 Hz, 1H, ArH), 7.85 (d, *J* = 8.1 Hz, 1H, ArH), 7.63 (d, *J* = 7.8 Hz, 1H, ArH), 7.60–7.55 (m, 1H, ArH), 7.46–7.49 (m, 2H, ArH), 7.40 (d, *J* = 8.2 Hz, 1H, ArH), 7.15 (bs, 2H, NH_2), 5.72 (s, 1H, CH); CHN ($C_{20}H_{13}ClN_2O$) calc. (%): C (72.18), H (3.90), N (8.42); found (%): C (72.01), H (3.71), N (8.24).

3-Amino-1-(4-chlorophenyl)-1*H*-benzo[*f*]chromene-2-carbonitrile (Entry 4):

White solid; M.p. 210 °C; IR (KBr, *v*, cm^{-1}): 3409, 3329, 2192, 1640, 1578, 1403, 1245, 1103, 1040, 803, 757; ^{1}H NMR (DMSO-d_6): δ 7.91 (d, *J* = 8.4 Hz, 1H, ArH), 7.52 (d, *J* = 8.3 Hz, 1H, ArH), 7.47–7.31 (m, 3H, ArH), 7.11 (d, *J* = 8.2 Hz, 2H, ArH), 6.99 (d, *J* = 8.5 Hz, 2H, ArH), 7.10 (d, *J* = 8.2 Hz, 1H, ArH), 7.02 (bs, 2H, NH_2), 5.38 (s, 1H, CH); CHN ($C_{20}H_{13}ClN_2O$) calc. (%): C (72.18), H (3.90), N (8.42); found (%): C (71.98), H (3.69), N (8.33).

3-Amino-1-(4-bromophenyl)-1*H*-benzo[*f*]chromene-2-carbonitrile (Entry 5):

White solid; M.p. 241 °C; IR (KBr, *v*, cm^{-1}): 3411, 3332, 2189, 1644, 1571, 1404, 1252, 1100, 1057, 802, 759; ^{1}H NMR (DMSO-d_6): δ 7.94–7.82 (m, 2H, ArH), 7.80–7.76 (m, 1H, ArH), 7.47–7.42 (m, 3H, ArH), 7.36–7.34 (m, 1H, ArH), 7.33–7.18 (m, 2H, ArH), 7.16 (d, *J* = 8.5 Hz, 1H, ArH), 7.03 (bs, 2H, NH_2), 5.36 (s, 1H, CH); CHN ($C_{20}H_{13}BrN_2O$) calc. (%): C (63.67), H (3.44), N (7.42); found (%): C (63.49), H (3.38), N (7.30).

3-Amino-1-(4-fluorophenyl)-1*H*-benzo[*f*]chromene-2-carbonitrile (Entry 6):

Light yellow solid; M.p. 234 °C; IR (KBr, *v*, cm^{-1}): 3411, 3333, 2192, 1636, 1573, 1400, 1251, 1103, 1041, 802, 757; ^{1}H NMR (DMSO-d_6): δ 7.95–7.91 (m, 2H, ArH), 7.91–7.82 (m, 1H, ArH), 7.46 (d, *J* = 6.5 Hz, 2H, ArH), 7.35–7.24 (m, 2H, ArH), 7.23 (d, *J* = 8.6 Hz, 1H, ArH), 7.11 (t, 2H, ArH), 7.00 (bs, 2H, NH_2), 5.34 (s, 1H, CH); CHN ($C_{20}H_{13}FN_2O$) calc. (%): C (75.94), H (4.11), N (8.86); found (%): C (75.52), H (4.08), N (8.49).

3-Amino-1-(*p*-tolyl)-1*H*-benzo[*f*]chromene-2-carbonitrile (Entry 7):

White solid; M.p. 183 °C, IR (KBr, *v*, cm-1): 3440, 3326, 2940, 2160, 1665, 1602, 1526, 1497, 1260, 1174, 1067, 742; ^{1}H NMR (DMSO-d_6): δ 7.90 (d, *J* = 7.1 Hz, 2H, ArH), 7.91–7.83 (m, 1H, ArH), 7.44 (d, *J* = 7.4 Hz, 2H, ArH), 7.36 (d, *J* = 8.2 Hz, 1H, ArH), 7.32–7.06 (m, 4H, ArH), 6.96 (bs, 2H, NH_2), 5.26 (s, 1H, CH), 2.21 (s, 3H, CH_3); CHN ($C_{21}H_{16}N_2O$) calc. (%): C (80.76), H (5.12), N (8.97); found (%): C (80.53), H (4.98), N (8.75).

3-Amino-1-(3-methoxyphenyl)-1*H*-benzo[*f*]chromene-2-carbonitrile (Entry 8):

White solid; M.p. 166 °C; IR (KBr, *v*, cm^{-1}): 3439, 3354, 2180, 1662, 1609, 1578, 1522, 1506, 1320, 1275, 1064, 761; ^{1}HNMR (DMSO-d_6): δ 8.04 (s, 1H, ArH), 8.00 (d, *J* = 8.3 Hz, 1H, ArH), 7.93 (d, *J* = 7.8 Hz, 1H, ArH), 7.91 (d, *J* = 7.5 Hz, 1H, ArH), 7.80 (d, *J* = 8.4 Hz, 1H, ArH), 7.65 (d, *J* = 7.3 Hz, 1H, ArH), 7.62–7.55 (m, 1H, ArH), 7.43–7.46 (m, 2H, ArH), 7.40 (d, *J* = 8.0 Hz, 1H, ArH), 7.19 (bs, 2H, NH_2), 5.72 (s, 1H, CH), 3.60 (s, 3H, OCH_3); CHN ($C_{21}H_{16}N_2O_2$) calc. (%): C (76.82), H (4.87), N (8.53); found (%): C (76.60), H (4.54), N (8.16).

3-Amino-1-(4-methoxyphenyl)-1*H*-benzo[*f*]chromene-2-carbonitrile (Entry 9):

Pale yellow solid; M.p. 181 °C; IR (KBr, *v*, cm^{-1}): 3422, 3317, 2978, 2170, 1662, 1605, 1521, 1504, 1295, 1232, 1185, 1079, 764; ^{1}H NMR (DMSO-d_6): δ 7.91 (d, *J* = 8.6 Hz, 2H, ArH), 7.63 (t, *J* = 7.6 Hz, 1H, ArH), 7.35–7.21 (m, 2H, ArH), 7.13 (d, *J* = 8.8 Hz, 1H, ArH), 7.02 (d, *J* = 8.0 Hz, 2H, ArH), 6.96 (d, *J* = 8.5 Hz, 2H, ArH), 6.82 (bs, 2H, NH_2), 5.27 (s, 1H, CH), 3.65 (s, 3H, OCH_3); CHN ($C_{21}H_{16}N_2O_2$) calc. (%): C (76.82), H (4.87), N (8.53); found (%): C (76.45), H (4.62), N (8.27).

3-Amino-1-(3-nitrophenyl)-1*H*-benzo[*f*]chromene-2-carbonitrile (Entry 10):

White solid; M.p. 233 °C; IR (KBr, *v*, cm^{-1}): 3440, 3357, 2181, 1661, 1601, 1576, 1520, 1502, 1322, 1277, 1065, 761; ^{1}HNMR (DMSO-d_6): δ 8.06 (s, 1H, ArH), 8.01 (d, *J* = 8.0 Hz, 1H, ArH), 7.96 (d, *J* = 7.6 Hz, 1H, ArH), 7.93 (d, *J* = 7.9 Hz, 1H, ArH), 7.83 (d, *J* = 8.2 Hz, 1H, ArH), 7.65 (d, *J* = 7.6 Hz, 1H, ArH), 7.61–7.57 (m, 1H, ArH), 7.45–7.48 (m, 2H, ArH), 7.41 (d, *J* = 8.5 Hz, 1H, ArH), 7.18 (bs, 2H, NH_2), 5.70 (s, 1H, CH); CHN ($C_{20}H_{13}N_3O_3$) calc. (%): C (69.97), H (3.79), N (12.24); found (%): C (69.70), H (3.31), N (12.07).

3-Amino-1-(4-nitrophenyl)-1*H*-benzo[*f*]chromene-2-carbonitrile (Entry 11):

White solid; M.p. 188 °C; IR (KBr, *v*, cm^{-1}): 3443, 3359, 2185, 1665, 1604, 1579, 1524, 1506, 1327, 1277, 1069, 766; ^{1}HNMR (DMSO-d_6): δ 7.94–7.95 (m, 2H, ArH), 7.95–7.83 (m, 1H, ArH), 7.50 (d, *J* = 6.0 Hz, 2H, ArH), 7.39–7.26 (m, 2H, ArH), 7.28 (d, *J* = 8.5 Hz, 1H, ArH), 7.15 (t, 2H, ArH), 7.02 (bs, 2H, NH_2), 5.35 (s, 1H, CH); CHN ($C_{20}H_{13}N_3O_3$) calc. (%): C (69.97), H (3.79), N (12.24); found (%): C (69.73), H (3.40), N (11.99).

3-Amino-1-(3-hydroxyphenyl)-1*H*-benzo[*f*]chromene-2-carbonitrile (Entry 12): White solid; M.p. 283 ºC; IR (KBr, *v*, cm^{-1}): 3411, 3333, 2192, 1636, 1573, 1400, 1251, 1103, 1041, 802, 757; ^{1}H NMR (DMSO-d_6): δ 5.33 (s, 1H, CH), 6.50 (t, J = 12.1 Hz, 2H, ArH), 6.62 (d, J = 7.1 Hz, 1H, ArH), 6.90 (s, 2H, NH2), 7.00 (t, J = 15.1 Hz, 1H, ArH), 7.35 (d, J = 8.5 Hz, 1H, ArH), 7.40–7.44 (m, 2H, ArH), 7.80 (d, J = 7.3 Hz, 1H, ArH), 7.90 (t, J = 8.1 Hz, 2H, ArH), 10.03 (s, 1H, OH); CHN ($C_{20}H_{14}N_2O_2$) calc. (%): C (76.43), H (4.45), N (8.91); found (%): C (76.21), H (4.34), N (8.75).

3-Amino-1-(4-hydroxyphenyl)-1*H*-benzo[*f*]chromene-2-carbonitrile (Entry 13): White solid; M.p. 292 ºC; IR (KBr, *v*, cm^{-1}): 3441, 3356, 2182, 1662, 1602, 1578, 1522, 1504, 1325, 1279, 1067, 763; ^{1}HNMR (DMSO-d_6): δ 7.96–7.92 (m, 2H, ArH), 7.93–7.84 (m, 1H, ArH), 7.49 (d, *J* = 6.2 Hz, 2H, ArH), 7.37–7.25 (m, 2H, ArH), 7.26 (d, *J* = 8.7 Hz, 1H, ArH), 7.13 (t, 2H, ArH), 7.03 (bs, 2H, NH_2), 5.37 (s, 1H, CH), 10.16 (s, 1H, OH), CHN ($C_{20}H_{14}N_2O_2$) calc. (%): C (76.43), H (4.45), N (8.91); found (%): C (76.16), H (4.19), N (8.62).

The spectra images of the some of the synthesized compounds are included in supplementary file for more information.

4. Conclusion

In this work, the $Yb_2V_2O_7$ nanomaterials were synthesized successfully via a low temperature and one step solid state method. PXRD analysis confirmed the successful synthesis of $Yb_2V_2O_7$ material. The Rietveld analysis showed that the reaction temperature played an important effect on the phase purity and crystal growth. FESEM image indicated that the as-synthesized nanomaterial had a mixture of sponge and circle morphologies. It was found that the reaction temperature had a main effect on the morphology of the nanomaterials obtained. $Yb_2V_2O_7$ was used as a reusable nanocatalyst for the fabrication of 2-amino-4H-chromene compounds under microwave irradiation. The maximum yield for the synthesis of the Chromene compounds was obtained (94%) when H_2O was used as reaction solvent, the catalyst amount, reaction time and temperature, and illumination frequency were (10 mol%), 12 min, 70 ˚C and 50 kHz, respectively, while benzaldehyde was used as aldehyde derivative.

Reference

[1] A.R. Cleave, Atomic scale simulations for waste form applications, in, University of London London, UK, 2006.

[2] J.B. Thomson, A.R. Armstrong and P.G. Bruce. J. Solid State Chem. 148, 56 (1999). https://doi.org/10.1006/jssc.1999.8347

[3] H. Kishimoto, T. Omata, S. Otsuka-Yao-Matsuo, K. Ueda, H. Hosono and H. Kawazoe. J. alloys compd. 312, 94-103 (2000). https://doi.org/10.1016/S0925-8388(00)01168-3

[4] D.J. Haynes, D.A. Berry, D. Shekhawat and J.J. Spivey. Catal. Today. 136, 206-213 (2008). https://doi.org/10.1016/j.cattod.2008.02.012

[5] R. Kieffer, M. Fujiwara, L. Udron and Y. Souma. Catal. today. 36, 15-24 (1997). https://doi.org/10.1016/S0920-5861(96)00191-5

[6] K. Matsuhira, M. Wakeshima, Y. Hinatsu and S. Takagi. J. Phys. Soc. Japan. 80, 094701 (2011). https://doi.org/10.1143/JPSJ.80.094701

[7] K. Ross, L. Yaraskavitch, M. Laver, J.S. Gardner, J. Quilliam, S. Meng, J. Kycia, D. Singh, T. Proffen and H. Dabkowska. Phys. Rev. B. 84, 174442 (2011). https://doi.org/10.1103/PhysRevB.84.174442

[8] Ziba Davtalab Nazarlou, Leila Kafi-Ahmadi, Shahin Khademinia. Journal of the Australian Ceramic Society https://doi.org/10.1007/s41779-021-00694-y .

[9] C. Shen, X. Tang, S.A. Cheema, C. Zhang, M.I. Khan, F. Liang, X. Chen, Y. Zhu, Q. Lin and Y. Chen. J. hazard. mater. 172, 1671-1676 (2009). https://doi.org/10.1016/j.jhazmat.2009.08.064

[10] J.K. Gill, O. Pandey and K. Singh. Solid State Sci. 13, 1960-1966 (2011). https://doi.org/10.1016/j.solidstatesciences.2011.08.025

[11] L. Soderholm, J. Greedan and M. Collins, J. Solid State Chem. 35, 385-390 (1980). https://doi.org/10.1016/0022-4596(80)90536-8

[12] L. Soderholm, The Magnetic Properties of the Series R2V2O7; R, 1982.

[13] T. Shin-Ike, G. Adachi and J. Shiokawa. Mater. Res. Bull. 12, 1149-1154 (1977). https://doi.org/10.1016/0025-5408(77)90168-4

[14] Z. Dun, J. Ma, H. Cao, Y. Qiu, J. Copley, T. Hong, M. Matsuda, J. Cheng, M. Lee and E. Choi. Phys. Rev. B. 91, 064425 (2015). https://doi.org/10.1103/PhysRevB.91.064425

[15] Kaminskii, A. A., Bagayev, S. N., Oka, K., Shibata, H., Ueda, K., Takaichi, K., ... & Rhee, H. (2006). Observation of stimulated Raman scattering in the tetragonal crystal YbVO4. *Laser Physics Letters*, *3*(5), 263. https://doi.org/10.1002/lapl.200510089

[16] Kaminskii, A. A., Eichler, H. J., Rhee, H., Ueda, K., Oka, K., & Shibata, H. (2008). New nonlinear-laser effects in YbVO 4 crystal: Sesqui-octave stokes and anti-Stokes comb generation and the cascaded self-frequency “tripling” of χ (3)-Stokes components under a one-micron picosecond pumping. *Laser physics*, *18*, 1546-1552. https://doi.org/10.1134/S1054660X08120268

[17] Hadilou, S., Behzad, M., & Khademinia, S. (2022). Solid state and hydrothermal synthesis,

characterization and optical properties of Yb2V2O7. *Progress in Physics of Applied Materials*, *2*(1), 63-69. https://doi.org/10.22075/ppam.2022.25660.1018

[19] Hutchison, W. D., Prandolini, M. J., Chaplin, D. H., Bowden, G. J., & Bleaney, B. (1996). A nuclear orientation study of YbVO4. *Czechoslovak Journal of Physics*, *46*(Suppl 4), 2151-2152. https://doi.org/10.1007/BF02571067

[20] Santos, C. C., Guedes, I., Loong, C. K., & Boatner, L. A. (2007). Low-temperature Raman spectra of YbVO4. *Vibrational Spectroscopy*, *45*(2), 95-98. https://doi.org/10.1016/j.vibspec.2007.05.002

[21] Xu, Z., Zhao, Q., Liu, T., Wang, L., & Bian, S. (2013). Uniform and well-dispersed YbVO4 hierarchical nanoarchitectures: synthesis and luminescence properties. *Journal of nanoscience and nanotechnology*, *13*(1), 344-350. https://doi.org/10.1166/jnn.2013.7083

[22] de Sousa Filho, P. C., Gacoin, T., Boilot, J. P., Walton, R. I., & Serra, O. A. (2015). Synthesis and luminescent properties of REVO4–REPO4 (RE= Y, Eu, Gd, Er, Tm, or Yb) heteronanostructures: a promising class of phosphors for excitation from NIR to VUV. *The Journal of Physical Chemistry C*, *119*(42), 24062-24074. https://doi.org/10.1021/acs.jpcc.5b08249

[23] Cheng, Y., Zhang, H., Zhang, K., Xin, Z., Yang, X., Xu, X., ... & Xu, J. (2009). Growth and spectroscopic characteristics of Er3+: YbVO4 crystal. *Journal of crystal growth*, *311*(15), 3963-3968. https://doi.org/10.1016/j.jcrysgro.2009.06.033

[24] Chakoumakos, B. C., Abraham, M. M., & Boatner, L. A. (1994). Crystal structure refinements of zircon-type MVO4 (M= Sc, Y, Ce, Pr, Nd, Tb, Ho, Er, Tm, Yb, Lu). *Journal of Solid State Chemistry*, *109*(1), 197-202. https://doi.org/10.1006/jssc.1994.1091

[25] Goudarzi, M., & Abedini, A. (2017). Synthesis, characterization, and investigation of magnetic and photocatalytic property of YbVO 4 nanoparticles. *Journal of Materials Science: Materials in Electronics*, *28*, 114-119. https://doi.org/10.1007/s10854-016-5499-9

[26] Z. Huang, L. Zhang and W. Pan. Inorg. chem., 51, 11235-11237 (2012). https://doi.org/10.1007/s10854-016-5499-9

[27] Kazei, Z. A., & Chanieva, R. I. (2006). Magnetoelastic effects in rare-earth vanadates YbVO 4 and HoVO 4. *Journal of Experimental and Theoretical Physics*, *102*, 266-276. https://doi.org/10.1134/S1063776106020087

[28] Das, B., Laxminarayana, K., Krishnaiah, M., & Srinivas, Y. (2007). An efficient and convenient protocol for the synthesis of novel 12-aryl-or 12-alkyl-8, 9, 10, 12-tetrahydrobenzo [a] xanthen-11-one derivatives. *Synlett*, *2007*(20), 3107-3112. https://doi.org/10.1055/s-2007-990922

[28] Li, J., Tang, W., Lu, L., & Su, W. (2008). Strontium triflate catalyzed one-pot condensation of β-naphthol, aldehydes and cyclic 1, 3-dicarbonyl compounds. *Tetrahedron Letters*, *49*(50), 7117-7120. https://doi.org/10.1016/j.tetlet.2008.09.129

[29] Khurana, J. M., & Magoo, D. (2009). pTSA-catalyzed one-pot synthesis of 12-aryl-8, 9, 10, 12-tetrahydrobenzo [a] xanthen-11-ones in ionic liquid and neat conditions. *Tetrahedron Letters*, *50*(33), 4777-4780. https://doi.org/10.1016/j.tetlet.2009.06.029

[30] Oskooie, H. A., Heravi, M. M., Karimi, N., & Kohansal, G. (2011). Cu/SiO2-catalyzed one-pot synthesis of 12-aryl-8, 9, 10, 12-tetrahydrobenzo [α] xanthen-11-ones under solvent-free conditions. *Synthetic Communications*, *41*(18), 2763-2768. https://doi.org/10.1080/00397911.2010.515353

[31] Lukasik, N., & Wagner-Wysiecka, E. (2014). A review of amide bond formation in microwave organic synthesis. *Current Organic Synthesis*, *11*(4), 592-604. https://doi.org/10.2174/1570179411666140321180857

[32] Frecentese F, Saccone I, Caliendo G, Corvino A, Fiorino F, Magli E, Perissutti E, Severino B, Santagada V. Microwave Assisted Organic Synthesis of Heterocycles in Aqueous Media: Recent Advances in Medicinal Chemistry. Medicinal Chemistry, 2016, 12(7).

[33] Jha, A. (2021). Microwave assisted synthesis of organic compounds and nanomaterials. In *Nanofibers-Synthesis, Properties and Applications*. IntechOpen. https://doi.org/10.5772/intechopen.98224

[34] Pascual, J., Camassel, J., & Mathieu, H. (1978). Fine structure in the intrinsic absorption edge of ti o 2. *Physical Review B*, *18*(10), 5606. https://doi.org/10.1103/PhysRevB.18.5606

[35] Ohmi, S., Kobayashi, C., Kashiwagi, I., Ohshima, C., Ishiwara, H., & Iwai, H. (2003). Characterization of La2 O 3 and Yb2 O 3 Thin Films for High-k Gate Insulator Application. *Journal of the Electrochemical Society*, *150*(7), F134. https://doi.org/10.1149/1.1581278

[36] Parker, J. C., Lam, D. J., Xu, Y. N., & Ching, W. Y. (1990). Optical properties of vanadium pentoxide determined from ellipsometry and band-structure calculations. *Physical Review B*, *42*(8), 5289. https://doi.org/10.1103/PhysRevB.42.5289

[37] Keshavarz, R., & Farahi, M. (2022). Novel cellulose supported 1, 2-bis (4-aminophenylthio) ethane Ni (ii) complex (Ni II (BAPTE)(NO 3) 2-

Cell) as an efficient nanocatalyst for the synthesis of spirooxindole derivatives. *RSC advances*, *12*(6), 3584-3592. https://doi.org/10.1039/d1ra08182a.

[38] H. Mehrabi, N. Kamali. J. Iran. Chemi. Soc. 9, 599 (2012). https://doi.org/10.1007/s13738-012-0073-8

[39] R. Maggi, R. Ballini, G. Sartori, Tetrahedron Lett. 45, 2297 (2004). https://doi.org/10.1016/j.tetlet.2004.01.115

[40] T.S. Jin, J.C. Xiao, S.J. Wang, T.S. Li, Ultrason. Sonochem. 11, 393 (2004). https://doi.org/10.1016/j.ultsonch.2003.10.002

[41] R. Teimuri-Mofrad, M. Gholamhosseini-Nazari, E. Payami and S. Esmati, Appl. Organomet. Chem. 32, 3955 (2018). https://doi.org/10.1002/aoc.3955

[42] D.S. Raghuvanshi, K.N. Singh, Arkivoc. *x*, 305 (2010). http://dx.doi.org/10.3998/ark.5550190.0011.a25.

[43] X.S. Wang, G.S. Yanga, G. Zhao, Tetrahedron. 19, 709 (2008). https://doi.org/10.1016/j.tetasy.2008.02.018

[44] L. Chen, C. Lin, Y., Lan, Z. Li, D. Huang, W. Yang, Y. Li (2020). Environmental Chemistry Letters, 18, 2157-2163 (2020). https://doi.org/10.1007/s10311-020-01053-2

[45] K. Gong, H.L. Wang, Z-L. Fang Liu. Catal. Commun. *9*, 650 (2008). https://doi.org/10.1016/j.catcom.2007.07.010

[46] S. Balalaie, S. Ramezanpour, M. Bararjanian, J.H. Gross, Synth. Commun. *38*, 1078 (2008). https://doi.org/10.1080/00397910701862865

[47] A.R. Moosavi-Zare, M.A. Zolfigol, O. Khaledian, V. Khakyzadeh, M.D. Farahani, M.H. Beyzavi, H.G. Kruger. Chem. Eng. J. 248, 122-127 (2014). https://doi.org/10.1016/j.cej.2014.03.035